Inorganic Chemistry

Article

pubs.acs.org/IC

Two-Step Antiferromagnetic Transitions and Ferroelectricity in Spin-1 Triangular-Lattice Antiferromagnetic $Sr_3NiTa_2O_9$

Meifeng Liu,*[,†] Huimin Zhang,[‡] Xin Huang,[‡] Chunyang Ma,[†] Shuai Dong,[‡] and Jun-Ming Liu*[,†,§]

[†]Laboratory of Solid State Microstructures and Innovative Center of Advanced Microstructures, Nanjing University, Nanjing 210093, China

[‡]Department of Physics, Southeast University, Nanjing 211189, China

[§]Institute for Advanced Materials and Laboratory of Quantum Engineering and Materials, South China Normal University, Guangzhou 510006, China

ABSTRACT: We report the low-temperature characterizations on structural, specific heat, magnetic, and ferroelectric behaviors of transition metal oxide compound $Sr_3NiTa_2O_9$. It is suggested that $Sr_3NiTa_2O_9$ is a spin-1 triangular lattice Heisenberg quantum antiferromagnet which may have weak easy-axis anisotropy. At zero magnetic field, a two-step transition sequence at T_{N1} = 3.35 K and T_{N2} = 2.74 K, respectively, is observed, corresponding to the up−up−down (uud) spin ordering and 120° spin ordering, respectively. The two transition points shift gradually with increasing magnetic field toward the low temperature, accompanying an evolution from the 120° spin structure (phase) to the normal oblique phases. Ferroelectricity in the 120° phase is clearly identified. The first-principles calculations confirm the 120° phase as the ground state whose ferroelectricity originates mainly from the electronic polarization.

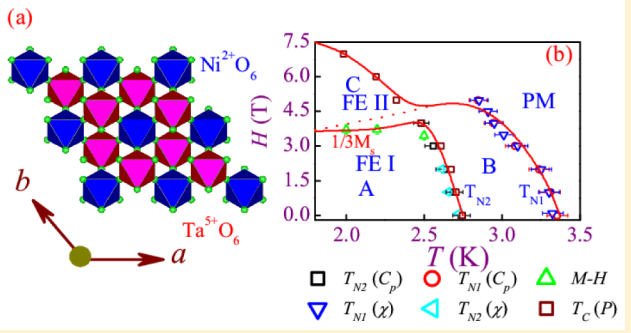

I. INTRODUCTION

Strongly correlated electron systems have been receiving attention over the past decades, in which frustrated quantum magnets represent a highly concerned class, owing to the rich variety of exotic quantum states and quantum spin frustration.[1−4] The most prominent examples include quantum spin liquids, spin ices, spin glasses, and noncollinear magnets.[3,5−7] It is recently recognized that noncollinear magnets may induce strong magnetoelectric coupling, as evidenced in a number of spiral spin ordered multiferroics.[8−12] These emergent quantum phenomena are believed to arise not only through the interplay of strong geometric frustration, low dimensionality, and small moment, but also via modulation using magnetic field (H). Although careful experimental investigations on these issue states have been reported, there remain some critical issues. For example, the ground state in these magnets as a controversial issue is still open.[13−16]

For antiferromagnetic triangle lattice Heisenberg spin systems where the small spin quantum number is $^1/_2$ or 1, an ordered *ab*-plane 120° ground state is believed, as shown in Figure 1a, qualitatively consistent with observations on classic triangle lattice Heisenberg spin systems.[17−20] Nevertheless, the ground state of triangle lattice Heisenberg antiferromagnet (TLAF) systems with small moment under a nonzero H is essentially determined by quantum fluctuation energy.[5,21,22] Theoretical predictions suggest that the *ab*-plane 120° ground state upon increasing H may be replaced by other quantum phases, characterized by magnetization (M) plateaus or anomalies against H. The one-third ($^1/_3$) plateau appears, corresponding to the *ab*-plane up−up−down (uud) state, as shown in Figure 1b in the low-H range, similar to the cases with the $^1/_3$ plateau in classic spin systems.[23,24] However, such a plateau has never been clearly identified in realistic quantum magnets, and instead a series of anomalies in the $M(H)$ dependence have been observed.[5,13,14,21] One of the reasons is associated with the failed attempt at growing high-quality single crystals.[13,14,25] Further enhanced H may drive the transition from the uud state to the oblique 2:1 canted spin state, shown in Figure 1c, and then to the ferromagnetic phase in the high-field range.[5,13,21,26] Such plateaus are not always available in classic spin systems, and in some cases the magnetic susceptibility χ (not M) as a function of H increases monotonously until magnetization saturation.[13,21,26−31]

In fact, quite a few of the TLAF systems have been investigated in past years, including $Ba_3NiNb_2O_9$,[13] $Ba_3CoNb_2O_9$,[14] and $Ba_3CoSb_2O_9$.[5,22] They all have high-symmetry layer-like structures, as shown in Figure 1d−f. The adjacent $Me^{2+}O_6$ and $Me^{5+}O_6$ octahedra with corner- or face-sharing are stacked, and magnetic ions (Me^{2+} = Ni^{2+} or Co^{2+}) are separated by nonmagnetic Me^{5+} (Nb, Sb, Ta, etc.) ions on the two-dimensional (*ab*) planes. For $Ba_3NiNb_2O_9$, sufficient H can drive the spin structure at low temperature (T) to evolve from the 120° phase to the uud phase, characterized by a

Received: October 4, 2015
Published: March 2, 2016

DOI: 10.1021/acs.inorgchem.5b02270
Inorg. Chem. 2016, 55, 2709−2716

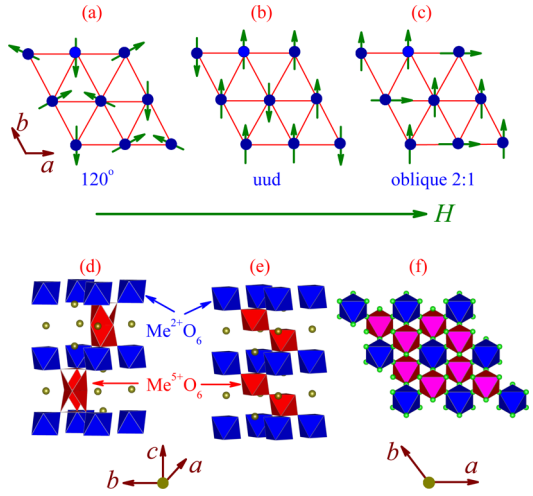

Figure 1. Schematic of magnetic structure: (a) the *ab*-plane 120° spin ground state under zero magnetic field, (b) the *ab*-plane up−up−down (uud) state in the low-*H* range, and (c) the oblique 2:1 canted spin state. Crystal structures of TLAF systems as schematically shown in parts d−f. The adjacent $Me^{2+}O_6$ and $Me^{5+}O_6$ octahedra with corner- or face-sharing are stacked, and magnetic ions (Me^{2+} = Ni^{2+} or Co^{2+}) are separated by nonmagnetic Me^{5+} (Nb, Sb, Ta, etc.) ions on the two-dimensional (*ab*) planes.

change of the $M(H)$ dependence slope (i.e., anomaly mentioned above) at $M = {}^1/_3M_s$ where M_s is the saturated magnetization, and eventually toward the oblique phase.[13] For $Ba_3CoSb_2O_9$, phase transitions occur in sequence at $M = {}^1/_3$, ${}^3/_5$, and ${}^2/_3M_s$, while the transitions appear at $M = {}^1/_3$, ${}^1/_2$, and ${}^2/_3M_s$ for $Ba_3CoNb_2O_9$, noting both systems have small Co^{2+} spin moment $S = {}^1/_2$.[5,14,22] Unfortunately, the origins for these magnetic transitions are not yet well-understood.

It is surprising to observe very different magnetic phase transitions in these structurally similar TLAF systems, raising the question of the structure−property relationships. Two issues deserve to be highlighted here. First, what is the reason for such big differences in the structure−property relationship? One may wonder how essential the quantum fluctuations associated with spin $S = {}^1/_2$ are in determining the ground state and phase transitions. The quantum fluctuations seem to be sensitive to the structural distortions which are different in, e.g., $Ba_3CoSb_2O_9$ and $Ba_3CoNb_2O_9$.[14,22] Do similar behaviors apply to another Ni^{2+} based TLAF system? So far, $Ba_3NiNb_2O_9$ has been well-investigated for these behaviors, while it would be interesting to address another Ni^{2+} based system with different Me^{5+} like Me = Ta. Second and in a more general sense, new quantum states in TLAF systems remain meaningful for materials chemistry and condensed matter physics, but so far available data are insufficient for drawing a conclusion on the underlying mechanism. It is not our motivation to address all these issues in this work; searching for more TLAF candidates that exhibit similar lattice structures but different magnetic properties is our major target.

Alternatively, another interesting issue is the possible multiferroicity observed in these TLAF systems. This issue is essentially motivated by magnetically induced ferroelectricity observed in a few triangle lattice AFM systems where the spin moments can be approximately treated as classic spins, such as $RbFe(MoO_4)_2$ ($S = {}^5/_2$) and $ACrO_2$ (A = Ag and Cu, $S = {}^3/_2$).[32,33] Due to the intensive studies on ferroelectricity in a number of noncollinear magnets,[34−36] the possible significance of discovering ferroelectricity in these quantum TLAF systems is straightforward. Here, the multiferroicity is mainly identified in noncollinear 120° spin states and the so-called Y state. The underlying mechanism for ferroelectricity in these spin systems is not yet fully understood, but the lattice distortion in coupling with the noncollinear spin structure is believed to be critical. In fact, several recent experiments did confirm the presence of nonzero ferroelectric polarization in TLAF sister structures such as $Ba_3NiNb_2O_9$ ($S = 1$), $Ba_3CoNb_2O_9$ ($S = {}^1/_2$), and $Ba_3MnNb_2O_9$ ($S = {}^5/_2$),[15] while the last one has a much bigger moment than the former two. However, for $Ba_3NiNb_2O_9$ and $Ba_3CoNb_2O_9$, both the collinear and noncollinear spin states exhibit ferroelectricity, while only the noncollinear spin state for approximately classic spin system $Ba_3MnNb_2O_9$ allows for the ferroelectricity which is absent in the collinear state.[15]

The above discussion on the TLAF systems constitutes the two sides of the coin for the present work. On one hand, $Ba_3CoSb_2O_9$ and $Ba_3CoNb_2O_9$, which have the same Co^{2+} ion but different Me^{5+} ions (Sb^{5+} and Nb^{5+}), exhibit different magnetic phase transitions.[14,22] $Ba_3NiNb_2O_9$ and $Ba_3CoNb_2O_9$, which have different magnetic Ni^{2+} and Co^{2+} ions but the same Me^{5+} ion, also show different magnetic behaviors.[13,14] One is then particularly interested in a search for an additional Ni based system which has another nonmagnetic Me^{5+} ion other than Nb^{5+}, in order to compare the magnetic behaviors with $Ba_3NiNb_2O_9$. On the other hand, one needs to check the one-to-one correspondence between the collinear/noncollinear spin structure and ferroelectricity. In this work, we report our investigation on a new member in this TLAF family: $Sr_3NiTa_2O_9$ (Ni^{2+} with $S = 1$ and Me^{5+} = Ta^{5+}), noting that Sr^{2+} is smaller than Ba^{2+} in ionic size and thus has slightly different lattice distortion between $Sr_3NiTa_2O_9$ and $Ba_3NiNb_2O_9$. It will be revealed that this compound is similar to $Ba_3CoNb_2O_9$ but different from $Ba_3NiNb_2O_9$ and $Sr_3NiNb_2O_9$[37] in terms of magnetic structure and phase transitions. It also shows two successive magnetic phase transitions into 120° spin ground state at $H = 0$. Furthermore, clear ferroelectricity is evidenced in the noncollinear 120° state.

II. EXPERIMENTAL DETAILS

Polycrystalline $Sr_3NiTa_2O_9$ samples were prepared using the conventional solid sintering method in air. The highly purified powder of oxides and carbonates was mixed in stoichiometric ratio, ground, and then fired at 1300 °C for 24 h. The resultant powder was reground and pelletized under a pressure of 1000 psi into disks of 2.0 cm in diameter, and then these pellets were sintered at 1400 °C for 24 h in air in prior to natural cooling down to room temperature. The sample crystallinity and microstructure were checked using X-ray diffraction (XRD) with the Cu Kα radiation at room temperature with an X-ray powder diffractometer (D8 Advanced, Bruker). The refinement of the XRD data was performed using the Rietveld method. The $\theta-2\theta$ XRD spectrum is plotted in Figure 2. It is shown that the trigonal $P\bar{3}m1$ space group with $a = 5.607$ Å and $b = 6.923$ Å can be well-fitted by the measured spectrum, as well-demonstrated in previous works on other Ba based and Sr based TLAF systems.[13,14] It is shown that the lattice structure model in Figure 1 can be applied to $Sr_3NiTa_2O_9$ too, where the Ni ions occupy the 1b Wyckoff sites and form the triangular lattice on the *ab*-plane, and the Ni magnetic triangular lattice occupations are separated by the two nonmagnetic Ta^{5+} layers. Therefore, $Sr_3NiTa_2O_9$ can be safely regarded as one member of the TLAF class.

The M as a function of T and H was measured using the Quantum Design superconducting quantum interference device magnetometer (SQUID) in the zero-field cooling (ZFC) and field-cooling (FC) modes, respectively. The specific heat C_p was measured from 2 to 300 K under H up to 9 T using a physical property measurement system

DOI: 10.1021/acs.inorgchem.5b02270
Inorg. Chem. 2016, 55, 2709−2716

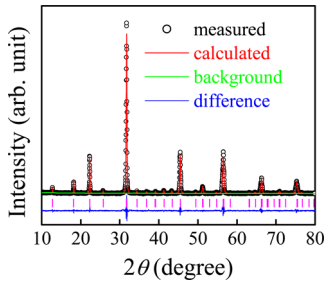

Figure 2. Rietveld refinement pattern for the powder X-ray diffraction data at room temperature.

(PPMS, Quantum Design) by the relaxation method. For electrical measurements, the disk-like samples of 3.0 mm in diameter and 0.2 mm in thickness were deposited with Au electrodes on the top/bottom surfaces. The dielectric constant ε as a function of T was measured using the HP4294A impedance analyzer attached to the PPMS. In our experiments, we used both Au and silver paste electrodes and observed no remarkable difference in terms of the dielectric response and pyroelectric current. The ferroelectric polarization P was measured by probing the zero-field pyroelectric current and isothermal polarized current via the Keithley 6514 electrometer connected with the PPMS too. For the pyroelectric current measurement, each sample was electrically poled under an electric field $E_p \sim 10$ kV/cm and cooled down from 50 to 2 K. Then, the poling field was removed, and the sample was electrically short-circuited for 40 min to several hours in order to exclude possible contributions other than the polarized charges associated with P. Usually, this discharging process continues until the background is less than 0.2 pA. The pyroelectric current I_{pyro} during the subsequent warming process was collected at different ramping rates of 0.5−2 K/min, respectively.

III. RESULTS AND DISCUSSION

3.1. Magnetic Behaviors. Figure 3a shows the dc magnetic susceptibilities $\chi(T)$ measured at $H \sim 0.1$ T over the whole T-range from 2 to 300 K. This field is believed to be sufficiently small. Here, several features deserve highlighting. First, no identifiable thermal hysteresis is observed between the ZFC and FC measurements. Second, the $\chi(T)$ curves demonstrate the Curie-like behavior in the high-T range, as shown in Figure 3a. Third, this rounded peak actually consists of two neighboring anomalies roughly at $T_{N1} \sim 3.35$ K and $T_{N2} \sim 2.74$ K, respectively, as defined by the $d\chi/dT$ as a function of T. Similar phenomena were reported in other TLAF systems,[25] in which the spin states below T_{N1} and T_{N2} were assigned as a collinear order and a 120° AFM phase. For the present system, all of the data indicate that the spin state below T_{N2} is also the 120° AFM phase, but the nature of the spin structure in $T_{N2} < T < T_{N1}$ remains unclear. The anomaly of $\chi(T)$ and $d\chi/dT$ at T_{N1} is insufficient to assign the oblique 2:1 phase. This spin state is most likely an up−up-down (uud) phase instead of an oblique 2:1 phase, and this issue will be discussed below, as shown in Figure 5.

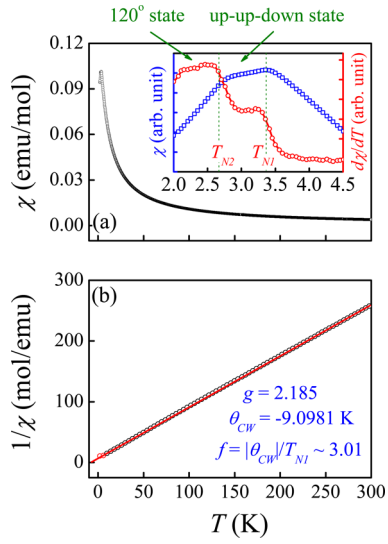

Figure 3. (a) Measured temperature dependence of magnetic susceptibility under $H = 0.1$ T. (b) The inverse magnetic susceptibility $1/\chi$ is fitted with the Curie−Weiss law $\chi = \chi_0 + C/(T + \theta_{CW})$ (red line). The inset in part a shows the corresponding $d(\chi)/dT$ at low temperature.

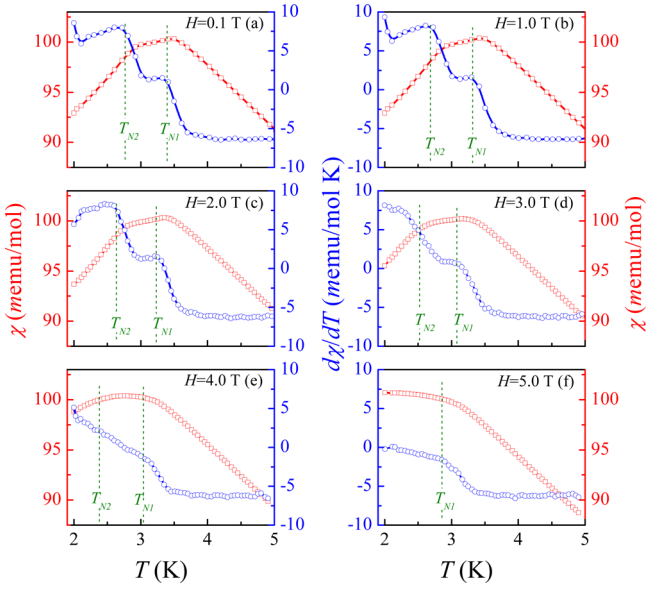

Figure 4. Measured $M(T)$ and $d(\chi)/dT$ under different H up to 5.0 T. The two-step transition sequence at T_{N1} and T_{N2} is labeled.

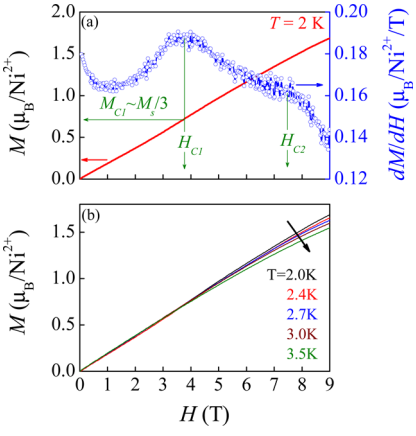

Figure 5. (a) Temperature dependence of magnetic susceptibility (left) and dM/dH (right) measured at 2 K. The arrows indicate the transitions explained in the text. (b) Field dependence of magnetization measured at different temperatures.

DOI: 10.1021/acs.inorgchem.5b02270
Inorg. Chem. 2016, 55, 2709−2716

Additionally, one may also argue that $Sr_3NiTa_2O_9$ is of weak axis anisotropy in terms of the two successive magnetic transitions at T_{N1} and T_{N2}.[5] It is this anisotropy that eventually drives the 120° phase below T_{N2}, fitted to the in-plane triangle lattice symmetry. In fact, it has been theoretically predicted that the easy-axis magnetic anisotropy favors a two-step magnetic ordering in a TLAF, consistent with our observations here.[38] Another TLAF system, $Ba_3NiSb_2O_9$, whose magnetic anisotropy is an easy-axis type, was reported to undergo two magnetic phase transitions at $T_{N1} \sim 13.5$ K and $T_{N2} \sim 13.0$ K.[39] Nevertheless, this argument still needs more checking from various aspects. First, due to the polycrystalline nature of our samples, a quantitative evaluation of this axis anisotropy is not yet possible for us. Second, there are several examples where Ni^{2+} in an octahedral environment leads to a small easy-plane anisotropy, e.g., in TLAF system $NiGa_2S_4$.[40] Also, for $Ba_3NiNb_2O_9$, the reported phase diagram is in striking agreement with theoretical expectation for an easy-plane anisotropy.[13]

Besides, the inverse $\chi^{-1}(T)$ data over a broad T-range plotted in Figure 3b can be fitted using the linear Curie−Weiss law $\chi = \chi_0 + C/(T + \theta_{CW})$, where C is the Curie constant, θ_{CW} is the Curie−Weiss temperature, and χ_0 is the T-independent contribution consisting of the diamagnetism from the core electron shells (core) and Van Vleck paramagnetism (χ_{VV}) of the open shells of Ni^{2+} ions. The fitting over the whole T-range gives $C = 1.189$ emu/(mol K) and $\theta_{CW} \sim -9.0981$ K < 0, suggesting the effective AFM interaction between Ni^{2+} ions. The estimated effective moment m_e is ~3.09 μ_B per Ni^{2+} ion, which corresponds to a Landé factor g of ~2.185, consistent with the nominal moment and g-factor value of 2.1−2.3 for the Ni^{2+} ion. In order to check this value for the Landé factor, we also performed the electron paramagnetic resonance (EPR) measurements on the sample from $T = 106$ K to room temperature. Unfortunately, the EPR measurement at lower T is inaccessible to us. From the relatively high-T data, the evaluated g value is ~2.11. It is expected that the high-T data should be slightly smaller than that predicted although this value does fall in the reasonable range.

In addition, the spin frustration ratio $f = |\theta_{CW}|/T_{N1}$ is ~3.01, indicating a moderate frustration in the system. This moderate frustration explains the nonidentifiable thermal hysteresis which should be serious otherwise in the strong frustration case. Surely, it should be mentioned that magnetization is a quantity related to the global spin arrangement, and a simple connection with individual spin moment (m_e) in the paramagnetic state may not be physically reasonable.

Furthermore, we investigate the $M(T)$ dependences under different H values, and the data are converted into a set of $\chi(T)$ curves under different H up to 5.0 T, plotted in Figure 4. Again, no thermal hysteresis is available for the data measured under the ZFC and FC conditions. Both T_{N1} and T_{N2} shift to lower T at higher field, although the anomalies in the $d\chi/dT$ curves become significantly broader at higher fields. The T_{N1} and T_{N2} (if any) determined from the $\chi \sim T$ and $d\chi/dT \sim T$ curves are in agreement with those obtained from the $C_P(T)$ data to be shown below. It is noted that similar features have been observed in $Ba_3CoNb_2O_9$,[14,25] $Li_2Co(WO_4)_2$,[41] and $Pb_3TeCoV_2O_{14}$.[42] Given the above argument that T_{N1} and T_{N2} mark, respectively, the transitions toward the uud phase and 120° phase, the three phases in sequence of decreasing T below $H \sim 4.0$ T are, respectively, the paramagnetic phase above T_{N1}, the uud phase between T_{N1} and T_{N2}, and the 120° phase below T_{N1}. It is predicted that field H essentially destabilizes the two ordered phases, which is a core characteristic of the TLAF systems evidenced so far.[5,13] The 120° phase seems to disappear at $H \sim 4.0$ T, which will be replaced by the normal oblique phase in the high-field range, to be discussed later.

We then look at the possible magnetic phase transitions upon varying H. We address the $M(H)$ data in the low-T range. In Figure 5a are shown the $M(H)$ data at $T = 2$ K, noting no isothermal field hysteresis in the H-cycle. A nearly linear $M(H)$ relationship is seen with no saturation tendency as H is up to 9.0 T. The largest M value at $H \sim 9.0$ T is only ~1.7 μ_B per Ni^{2+} ion, still smaller than the estimated saturated value M_s corresponding to $gS \sim 2.185$ μ_B per Ni^{2+} ion for $Sr_3NiTa_2O_9$, suggesting the nature of strong AFM interactions in this compound. Nevertheless, one is still able to detect magnetic phase transitions by looking into the details of $M(H)$ dependence. The plotted dM/dH data as a function of H at $T = 2$ K are shown in Figure 5a, too. One sees two anomalies, respectively, at $H_{C1} \sim 3.8$ T and $H_{C2} \sim 7.3$ T. The existence of the peak at H_{C1} supports the assignment of 120° phase below H_{C1}. Furthermore, the corresponding magnetization M_{C1} is ~0.7 μ_B, and the estimated M_{C1}/M_s ratio is ~0.32, marking the appearance of the $^1/_3$ plateau, again consistent with the assignment of 120° phase below T_{N1} and below H_{C1}.

Unfortunately, the anomaly at H_{C2} is not a peak but a weak shoulder, suggesting the appearance of a normal oblique phase between H_{C1} and H_{C2}. This makes an identification of the transition at H_{C1} unsure. Most likely, an H-driven transition from the 120° phase to the normal oblique phase occurs at $H \sim H_{C1}$. Furthermore, the measured $M(H)$ data at several T up to 3.5 K are plotted in Figure 5b. Both the H_{C1} and H_{C2} determined from the H-derivative of M data shift to the lower magnetic fields at higher T, although the peak at H_{C1} and the shoulder at H_{C2} become weaker and smeared above ~2.7 K. Here it should be mentioned that the magnetization does not saturate until 9 T, implying that higher field experiments are needed.

3.2. Specific Heat. The specific heat C_P under various H over broad T-range can also provide information on the magnetic phase transitions, and in particular at such low temperature the magnetic contribution to the specific heat would be dominant, and the phononic contribution is minor, to be discussed right below. As an example, the C_P/T data at $T = 2$ K under zero field are plotted in Figure 6a. The rapid rising C_P/T with decreasing T in the low-T range reflects the significant contribution from the magnetic ordering. Two successive peaks also at $T_{N1} \sim 3.3$ K and $T_{N2} \sim 2.7$ K are observed, consistent with the indications from the $M(T)$ data.

For a detailed analysis, one considers the magnetic and phonon contributions due to the fact that $Sr_3NiTa_2O_9$ is a magnetic insulator. First, the C_P/T values around ~10 K are close to zero, suggesting that the phonon contribution is sufficiently weak as T is down to ~10 K, and the specific heat below ~10 K is mainly from the magnetic ordering.[25] The magnetic entropy S obtained by integrating the C_P/T data below ~10 K gives $S_{mag} \sim 0.92R \ln 3$, close to the standard estimation $S_{mag} = nR \ln(2S + 1) \sim 9.136$ J/(mol K), where n is the number of magnetic ions in one unit cell ($n = 1$ for $Sr_3NiTa_2O_9$). The corresponding entropy gains at T_{N1} and T_{N2} are ~$0.43S_{mag}$ and ~$0.26S_{mag}$, respectively. In addition, one finds that the specific heat values between 2 and 2.7 K are well-fitted by the power law $C_P = AT^2$, where $A \sim 1.397$ is a

DOI: 10.1021/acs.inorgchem.5b02270
Inorg. Chem. 2016, 55, 2709−2716

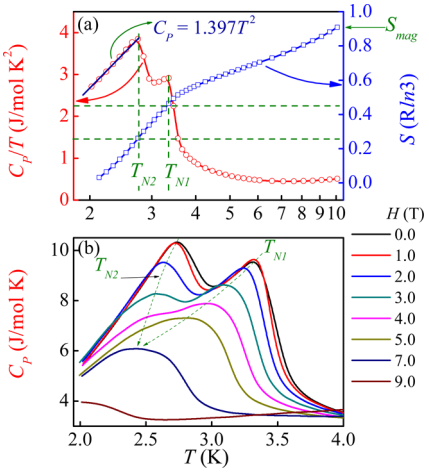

Figure 6. (a) Temperature dependence of specific heat (C_P) at zero fields (left) and magnetic entropy (S_{mag}) (right). The blue solid line shows the T^2 dependence of C_P. (b) Temperature dependence of specific heat (C_P) under different H up to 9.0 T.

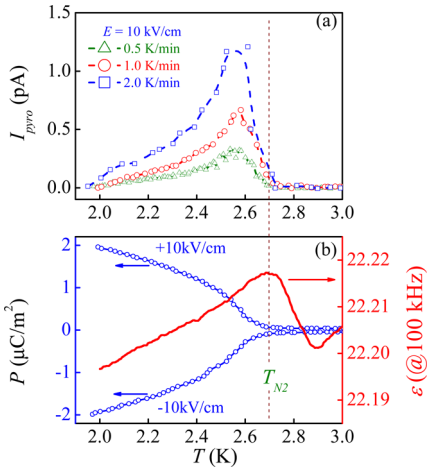

Figure 7. (a) Measured pyroelectric current I as a function of T at three warming rates 0.5, 1.0, and 2.0 K/min, respectively. (b) The FE polarizations under positive and negative poling electric fields (left) and the dielectric constant (ε, right axis) vs T.

constant. This power law indicates that $Sr_3NiTa_2O_9$ can be regarded as a pseudo-two-dimensional triangular magnet, i.e., the Ni magnetic triangular lattices are magnetically separated by the two nonmagnetic Ta layers.[43] The remaining spin entropy is from the gradually enhanced short-range magnetic correlation over a broad T-range above T_{N1}.

On the other hand, the measured $C_P(T)$ data under different fields up to 9 T demonstrate the evolution of the magnetic phase transitions upon increasing H, as shown in Figure 6b. The evolutions of the two transition points T_{N1} and T_{N2}, as indicated by the dashed arrows, evidence the shift toward the low-T side on one hand and gradually suppressed peak magnitudes on the other hand. The broad peak in the specific heat at 7 T is not a phase transition, but a development of short-range order in the triangular plane. These results are similar to the observations on the other systems with two AFM magnetic transitions.[25] Further increasing H makes the two peaks merge into one broad peak, also indicating that the interplanar interaction is suppressed by magnetic field, consistent with the magnetic susceptibility data. In short, the peak-merging is believed to mark the order−disorder transition induced by an intermediate magnetic field.

3.3. Ferroelectric Polarization. Now, we focus on the ferroelectric and dielectric behaviors. As an example, we show the measured pyroelectric current I_{pyro} as a function of T under $H = 0$ in Figure 7a. Three different warming rates (0.5, 1.0, and 2.0 K/min) are chosen, and the measured current peaks at the three warming rates appear roughly at the same temperature without much shift, demonstrating that the measured signals do come from the pyroelectric current. It is seen that nonzero I_{pyro} appears roughly at T_{N2}, suggesting the intrinsic correlation of the current with the 120° spin state, while the normal oblique phase may be weakly ferroelectric if at all. We also measure the I_{pyro} data under the positive and negative pooling electrical field E = 1000 kV/m, respectively, and the dielectric constant $\varepsilon(T)$ at a frequency of 100 kHz and the evaluated polarization $P(T)$ data are plotted in Figure 7b. The dielectric anomaly coincides with the initiation point of the $P(T)$ at T_{N2}. The symmetrical $P(T)$ curves upon the positive/negative poling fields suggest that the polarization can be reversed electrically. More important is that the ferroelectric transition begins roughly below T_{N2}, and the P value at $T \sim 2.0$ K is ~2 μC/m^2. The maximal P value is similar to that of $Ba_3NiNb_2O_9$[13] and $Ba_3CoNb_2O_9$.[14] These results suggest that the ferroelectricity appears in the 120° spin state.

Given the hypothesis that the ferroelectricity is related to the specific magnetic structure, one would expect that the polarization P is highly H-dependent. Therefore, a series of $I_{pyro}(T)$ curves measured at 1 K/min warming rate under the isofield conditions are obtained, and the data are plotted in Figure 8a. The evaluated $P(T)$ data under these fields are plotted in Figure 8b. Several features deserve highlighting here. First, the I_{pyro} peak shifts toward the low-T side with increasing H and the evaluated peak positions coincide roughly with the T_{N2} instead of T_{N1} as determined from the C_P/T data and dM/dT data, demonstrating the magnetic nature of the ferroelectricity. Second, the one-to-one correspondence between the ferroelectric transition points and T_{N2} for all the cases suggests once more that the 120° spin state is ferroelectricity-active. Third, the gradual magnitude suppression and peak-shifting of $I_{pyro}(T)$ dependence upon increasing H further confirm the magnetic nature of ferroelectricity. However, the polarization suppression by magnetic field is not yet completed until $H \sim H_{C2} \gg H_{C1}$, implying that the normal oblique phase may be also ferroelectricity-active but the ferroelectricity is quite weak. To illustrate the ferroelectric response, the evaluated P and magnetoelectric response ME = $[P(H = 0) - P(H)]/P(H = 0)$ at three temperatures are plotted in Figure 8c. It is noted that the polarization is seriously suppressed by increasing H. At T = 2 K, the ME response is up to 90% at H = 7 T, indicating the strong magnetoelectric coupling. From a comparison with the specific heat data and magnetic susceptibility data in response to magnetic field across H = 7 T, it is suggested that the normal oblique phase has no magnetic field induced ferroelectricity.

IV. DISCUSSION

4.1. Phase Diagram. To this stage, a multiferroic phase diagram for $Sr_3NiTa_2O_9$ from all the measured data on $M(T, H)$, $C_P(T, H)$, and $P(T, H)$ can be proposed, as shown in Figure 9a, although not all the phase boundaries are sufficiently apparent with small uncertainties. Three magnetic phases in addition to the paramagnetic (PM) phase are proposed, similar

DOI: 10.1021/acs.inorgchem.5b02270
Inorg. Chem. 2016, 55, 2709−2716

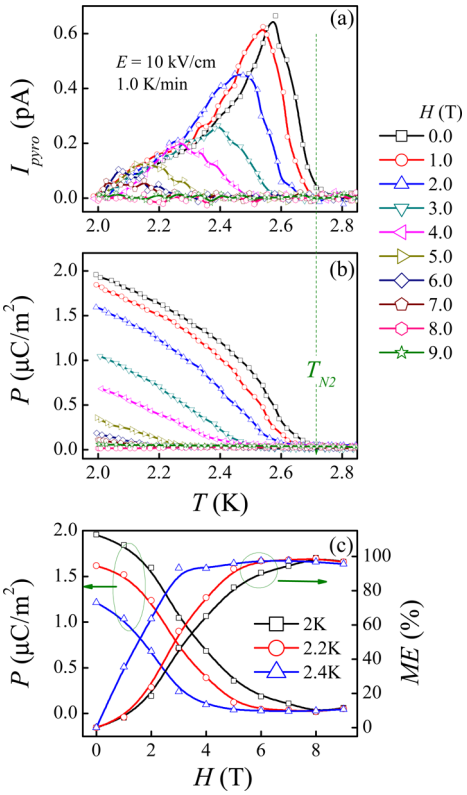

Figure 8. Measured (a) I_{pyro}–T data and (b) P–T data under various magnetic fields. (c) Evaluated P–H and ME (%)–H relations under 2, 2.2, and 2.4 K.

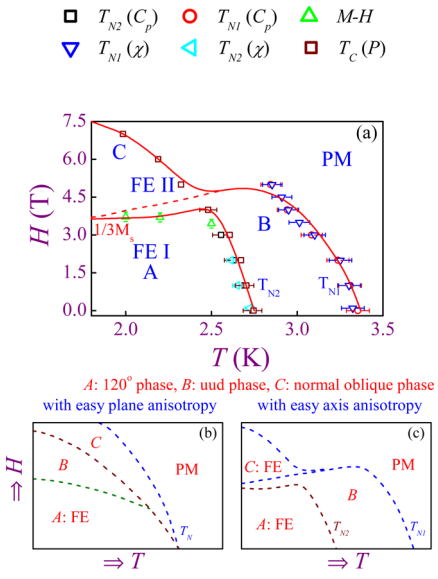

Figure 9. (a) Phase diagram constructed from data of magnetic susceptibility χ, magnetization M, specific heat C_P, and polarization P as a function of T and H. The 120° spin phase (A phase), uud phase (B phase), and normal oblique phase (C phase) are labeled. Here it is noted that the dashed boundary between B and C indicates that the normal oblique phase is only weakly ferroelectric if at all. The TLAF systems with easy-plane anisotropy and easy-axis anisotropy are as schematically shown in parts b and c.

to other TLAF systems with active ferroelectricity.[14] They are the 120° spin phase (A phase), the uud spin phase (B phase), and the normal oblique phase (C phase). Here the boundary (dashed line) between regions B and C indicates that the normal oblique phase is weakly ferroelectric. In fact, details on this boundary remain unclear. First, the two-step transitions at T_{N1} = 3.35 K and T_{N2} = 2.74 K under H = 0 coincide with theoretically predicted two-step magnetic transitions for a TLAF system with the easy-axis anisotropy, as schematically shown in Figure 9c.[44,45] Second, but differently, a direct and single-step transition was identified for other TLAF systems with the easy-plane anisotropy, and in fact the absence of the uud spin phase at H = 0 was believed for a Heisenberg model with isotropic or easy-plane anisotropy,[44,45] as schematically shown in Figure 9b. By contrast, the easy-axis exchange anisotropy and easy-axis single-ion anisotropy were believed to stabilize the uud phase at H = 0.[24,38,46−48] Here, $Sr_3NiTa_2O_9$ enters the uud phase and then the 120° phase upon cooling. $Sr_3NiTa_2O_9$ may be an exception which has the easy-axis anisotropy uud phase between the 120° phase and normal oblique phase.

More interestingly, we have found that the 120° phase is ferroelectric, while the ferroelectricity of the normal oblique phase needs additional checking, and it is weak if there is any. To our best knowledge, magnetically induced ferroelectricity has been observed in quite a few TLAF systems, such as $RbFe(MoO_4)_2$ ($S = {}^5/_2$), $ACrO_2$ (A = Ag and Cu, $S = {}^3/_2$), and $Ba_3NiNb_2O_9$ (S = 1).[13,32,49] The ferroelectricity of $ACrO_2$ comes from the Cr^{3+} ($S = {}^3/_2$) spiral spin order.[33] For $RbFe(MoO_4)_2$, the space group below 180 K is $P\bar{3}m$, and the nearest neighbor layers favor the AFM alignment while the in-plane magnetic order favors the 120° phase as the ground state at H = 0.[32] The absence of a mirror plane perpendicular to the c-axis and the broken inversion symmetry seem to drive the ferroelectric polarization in the 120° phase (or Y state).[13,32] This mechanism may be used to understand the origin for ferroelectricity in $Sr_3NiTa_2O_9$ at the 120° phase. However, the weak ferroelectricity if any in the normal oblique phase requires further studies for clarification. Here we perform the first-principles calculations on the magnetic structure in order to provide additional data on the origin of ferroelectricity in the 120°-phase.

4.2. First-Principles Calculations. Our first-principles calculations are based on the density functional theory (DFT), and are performed using the projector-augmented wave (PAW) potentials as implemented in the Vienna ab initio simulation package (VASP).[50,51] The electron interactions are described using the PBEsol (Perdew–Burke–Ernzerhof-revised) parametrization of the generalized gradient approximation (GGA). We started from experimentally determined lattice structure and symmetry, and the atomic positions and lattice constants are fully optimized iteratively until the Hellman–Feynman forces converged to be less than 0.01 eV/Å. The plane-wave cutoff is set to be 525 eV, and 4 × 4 × 5 Monkhorst–Pack k-point mesh centered at the Γ point is adopted. The polarization is calculated using the standard Berry phase method.

We first discuss the magnetic ground state. After the lattice relaxation was performed under the ferromagnetic condition, several possible magnetic orders have been tested, including ferromagnetic (FM), 120°-noncollinear, uud-collinear, and oblique phases. The DFT calculations show that the 120° noncollinear order has the lowest energy. Taking this energy as a reference (zero), the energy values for the FM, uud, and oblique phases are 10.5, 2.9, and 45.0 meV per unit, respectively, implying that the 120°-noncollinear order is the

DOI: 10.1021/acs.inorgchem.5b02270
Inorg. Chem. 2016, 55, 2709−2716

ground state. By mapping the system to a classical spin model and comparing the energies of various magnetic states, the nearest-neighbor exchange coupling of Ni is estimated to be 0.7 meV, which implies a weak exchange coupling.

With the 120°-noncollinear order, the calculated density of states (DOS) for $Sr_3NiTa_2O_9$ and its projected density of states (PDOS) to each atom are plotted in Figure 10a,b, respectively.

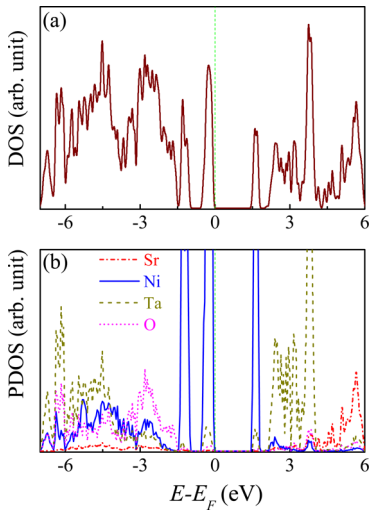

Figure 10. (a) Total density of states (DOS) and (b) atomic-resolved DOS.

It is seen from the DOS data that $Sr_3NiTa_2O_9$ is a Mott insulator with a moderate bandgap of ~1.40 eV. The PDOS data present more information on the contributions of Sr^{2+}, Ni^{2+}, Ta^{5+}, and O^{2-} to the band structure. The valence band maximum (VBM) and conductive band minimum (CBM) are mainly occupied with the 3d e_g-electrons of Ni^{2+}. The 2p electrons of O^{2-}, 3d electrons of Ni^{2+}, and 5d electrons of Ta^{5+} distribute over the whole region from −7.0 to −1.5 eV, indicating strong p−d hybridization. A minor contribution from the 5d electrons of Ta^{5+} to the VBM and CBM is also found, suggesting the existence of O-bridged superexchange between Ni^{2+} and Ta^{5+}.

Given the in-plane 120° spin state, the Berry phase calculation considering the spin−orbit coupling yields a ferroelectric polarization of ~49.86 $\mu C/m^2$ along the c-axis. Further carefully relaxed (with spin−orbit coupling, 120° spin order, and higher accuracy) atomic positions give a polarization of 45.63 $\mu C/m^2$, which is very close to above value obtained using the high-symmetry structure. Therefore, one is allowed to argue that the polarization is mainly from electronic contribution while the ionic component if any is weak. This electronic polarization is associated with the absence of a mirror plane perpendicular to the c-axis and the broken inversion symmetry in the 120° phase. Although the calculated value seems to be larger than the measured polarization ~2.0 $\mu C/m^2$, it remains quite reasonable considering the polycrystalline sample and the nonsaturable pyroelectricity. The origin for observed polarization in the magnetic field driven uud phase remains to be investigated.

It should be mentioned that the measured polarization is far smaller than the first-principles calculated value. This is probably a common concern for most comparisons of experimental data with theoretical predictions based on first-principles regarding most multiferroics with magnetic origin for polarization. For most multiferroics except $BiFeO_3$, first-principles usually predict much larger polarization than the measured value.[52,53] The polarization of polycrystalline samples for these multiferroics is also several times smaller than that of single crystals.[54,55] Our data are from the pyroelectric current method which does not allow measurement under electric bias. The measured value is thus only the remnant polarization instead of the saturated value, given sufficient electric poling which is actually inaccessible in our experiments performed in a PPMS system at such a low temperature.

To this end, we have established the one-to-one correspondence between the magnetic transitions and ferroelectricity in $Sr_3NiTa_2O_9$, and also found several features inconsistent with observations in similar TLAF systems. Since the Ni^{2+} moment is $S = 1$, it is reasonable to expect strong quantum fluctuations which compete with the exchanges. This competition may also be highly sensitive to subtle variations of chemical species, lattice distortion, and spin−orbit coupling, etc. Therefore, scattered magnetic and ferroelectric behaviors can be observed in structurally similar TLAF systems with small magnetic moment. $Sr_3NiTa_2O_9$ represents an additional system in this category.

V. CONCLUSION

In conclusion, we have investigated the magnetic phase transitions and multiferroic behaviors in a novel TLAF compound $Sr_3NiTa_2O_9$. It is revealed that $Sr_3NiTa_2O_9$ exhibits two successive magnetic transitions at T_{N1} = 3.35 K and T_{N2} = 2.74 K, respectively, from the paramagnetic state to the uud state and then to the 120° state. The 120° ground state may be replaced by the normal oblique state upon increasing magnetic field up to ~3.8 and ~7.0 T, respectively. These results suggest that $Sr_3NiTa_2O_9$ may have weak easy-axis anisotropy. Interestingly, it is observed that 120° phase and normal oblique phase are ferroelectric with remarkable magnetoelectric response. The ferroelectric polarization in the 120° phase aligns along the c-axis and originates from electronic contribution.

AUTHOR INFORMATION

Corresponding Authors

*E-mail: lmfeng1107@163.com (M.F.).
*E-mail: liujm@nju.edu.cn (J.-M.L.).

Notes

The authors declare no competing financial interest.

ACKNOWLEDGMENTS

The authors would like to thank the second referee for his/her stimulating suggestion. This work was supported by the National Natural Science Foundation of China (Grant Nos. 11374147, 11234005, 51332006, 51322206) and the National Basic Research Program of China (Grant No. 2015CB654602).

REFERENCES

(1) Anderson, P. W. *Mater. Res. Bull.* **1973**, *8*, 153−160.
(2) Balents, L. *Nature* **2010**, *464*, 199−208.
(3) Kalmeyer, V.; Laughlin, R. B. *Phys. Rev. Lett.* **1987**, *59*, 2095−2098.
(4) Lee, P. A. *Science* **2008**, *321*, 1306−1307.
(5) Susuki, T.; Kurita, N.; Tanaka, T.; Nojiri, H.; Matsuo, A.; Kindo, K.; Tanaka, H. *Phys. Rev. Lett.* **2013**, *110*, 267201.
(6) Gingras, M. J. P.; McClarty, P. A. *Rep. Prog. Phys.* **2014**, *77*, 056501.

DOI: 10.1021/acs.inorgchem.5b02270
Inorg. Chem. 2016, 55, 2709−2716

(7) LaForge, A. D.; Pulido, S. H.; Cava, R. J.; Chan, B. C.; Ramirez, A. P. *Phys. Rev. Lett.* **2013**, *110*, 017203.
(8) Hemberger, J.; Schrettle, F.; Pimenov, A.; Lunkenheimer, P.; Ivanov, V. Y.; Mukhin, A. A.; Balbashov, A. M.; Loidl, A. *Phys. Rev. B: Condens. Matter Mater. Phys.* **2007**, *75*, 035118.
(9) Kimura, T.; Lawes, G.; Goto, T.; Tokura, Y.; Ramirez, A. P. *Phys. Rev. B: Condens. Matter Mater. Phys.* **2005**, *71*, 224425.
(10) Amuneke, N. E.; Tapp, J.; de la Cruz, C. R.; Möller, A. *Chem. Mater.* **2014**, *26*, 5930−5935.
(11) Wang, K. F.; Liu, J. M.; Ren, Z. F. *Adv. Phys.* **2009**, *58*, 321−448.
(12) Dong, S.; Liu, J.-M.; Cheong, S.-W.; Ren, Z. *Adv. Phys.* **2015**, *64*, 519−626.
(13) Hwang, J.; Choi, E. S.; Ye, F.; Dela Cruz, C. R.; Xin, Y.; Zhou, H. D.; Schlottmann, P. *Phys. Rev. Lett.* **2012**, *109*, 257205.
(14) Lee, M.; Hwang, J.; Choi, E. S.; Ma, J.; Dela Cruz, C. R.; Zhu, M.; Ke, X.; Dun, Z. L.; Zhou, H. D. *Phys. Rev. B: Condens. Matter Mater. Phys.* **2014**, *89*, 104420.
(15) Lee, M.; Choi, E. S.; Huang, X.; Ma, J.; Dela Cruz, C. R.; Matsuda, M.; Tian, W.; Dun, Z. L.; Dong, S.; Zhou, H. D. *Phys. Rev. B: Condens. Matter Mater. Phys.* **2014**, *90*, 224402.
(16) Yang, M.; Zhang, S.-Y.; Guo, W.-B.; Tang, Y.-Y.; He, Z.-Z. *Dalton Transactions* **2015**, *44*, 15396−15399.
(17) Huse, D. A.; Elser, V. *Phys. Rev. Lett.* **1988**, *60*, 2531−2534.
(18) Jolicoeur, T.; Le Guillou, J. C. *Phys. Rev. B: Condens. Matter Mater. Phys.* **1989**, *40*, 2727−2729.
(19) Bernu, B.; Lecheminant, P.; Lhuillier, C.; Pierre, L. *Phys. Rev. B: Condens. Matter Mater. Phys.* **1994**, *50*, 10048−10062.
(20) Singh, R. R. P.; Huse, D. A. *Phys. Rev. Lett.* **1992**, *68*, 1766−1769.
(21) Ono, T.; Tanaka, H.; Aruga Katori, H.; Ishikawa, F.; Mitamura, H.; Goto, T. *Phys. Rev. B: Condens. Matter Mater. Phys.* **2003**, *67*, 104431.
(22) Shirata, Y.; Tanaka, H.; Matsuo, A.; Kindo, K. *Phys. Rev. Lett.* **2012**, *108*, 057205.
(23) Svistov, L. E.; Smirnov, A. I.; Prozorova, L. A.; Petrenko, O. A.; Demianets, L. N.; Shapiro, A. Y. *Phys. Rev. B: Condens. Matter Mater. Phys.* **2003**, *67*, 094434.
(24) Ishii, R.; Tanaka, S.; Onuma, K.; Nambu, Y.; Tokunaga, M.; Sakakibara, T.; Kawashima, N.; Maeno, Y.; Broholm, C.; Gautreaux, D. P.; Chan, J. Y.; Nakatsuji, S. *Europhys. Lett.* **2011**, *94*, 17001.
(25) Yokota, K.; Kurita, N.; Tanaka, H. *Phys. Rev. B: Condens. Matter Mater. Phys.* **2014**, *90*, 014403.
(26) Alicea, J.; Chubukov, A. V.; Starykh, O. A. *Phys. Rev. Lett.* **2009**, *102*, 137201.
(27) Nishimori, H.; Miyashita, S. *J. Phys. Soc. Jpn.* **1986**, *55*, 4448−4455.
(28) Chubokov, A. V.; Golosov, D. I. *J. Phys.: Condens. Matter* **1991**, *3*, 69.
(29) Farnell, D. J. J.; Zinke, R.; Schulenburg, J.; Richter, J. *J. Phys.: Condens. Matter* **2009**, *21*, 406002.
(30) Fortune, N. A.; Hannahs, S. T.; Yoshida, Y.; Sherline, T. E.; Ono, T.; Tanaka, H.; Takano, Y. *Phys. Rev. Lett.* **2009**, *102*, 257201.
(31) Sakai, T.; Nakano, H. *Phys. Rev. B: Condens. Matter Mater. Phys.* **2011**, *83*, 100405.
(32) Kenzelmann, M.; Lawes, G.; Harris, A. B.; Gasparovic, G.; Broholm, C.; Ramirez, A. P.; Jorge, G. A.; Jaime, M.; Park, S.; Huang, Q.; Shapiro, A. Y.; Demianets, L. A. *Phys. Rev. Lett.* **2007**, *98*, 267205.
(33) Kimura, K.; Nakamura, H.; Ohgushi, K.; Kimura, T. *Phys. Rev. B: Condens. Matter Mater. Phys.* **2008**, *78*, 140401.
(34) Kimura, T.; Goto, T.; Shintani, H.; Ishizaka, K.; Arima, T.; Tokura, Y. *Nature* **2003**, *426*, 55−58.
(35) Chapon, L. C.; Blake, G. R.; Gutmann, M. J.; Park, S.; Hur, N.; Radaelli, P. G.; Cheong, S. W. *Phys. Rev. Lett.* **2004**, *93*, 177402.
(36) Taniguchi, K.; Abe, N.; Takenobu, T.; Iwasa, Y.; Arima, T. *Phys. Rev. Lett.* **2006**, *97*, 097203.
(37) Lee, M.; Choi, E.; Zhou, H. *National High Magnetic Field Laboratory Maglab Research Report*; 2013
(38) Kawamura, H.; Miyashita, S. *J. Phys. Soc. Jpn.* **1985**, *54*, 4530−4538.
(39) Shirata, Y.; Tanaka, H.; Ono, T.; Matsuo, A.; Kindo, K.; Nakano, H. *J. Phys. Soc. Jpn.* **2011**, *80*, 093702.
(40) Nakatsuji, S.; Nambu, Y.; Onoda, S. *J. Phys. Soc. Jpn.* **2010**, *79*, 011003.
(41) Muthuselvam, I. P.; Sankar, R.; Ushakov, A. V.; Rao, G. N.; Streltsov, S. V.; Chou, F. C. *Phys. Rev. B: Condens. Matter Mater. Phys.* **2014**, *90*, 174430.
(42) Markina, M. M.; Mill, B. V.; Zvereva, E. A.; Ushakov, A. V.; Streltsov, S. V.; Vasiliev, A. N. *Phys. Rev. B: Condens. Matter Mater. Phys.* **2014**, *89*, 104409.
(43) Nakatsuji, S.; Nambu, Y.; Tonomura, H.; Sakai, O.; Jonas, S.; Broholm, C.; Tsunetsugu, H.; Qiu, Y.; Maeno, Y. *Science* **2005**, *309*, 1697−1700.
(44) Matsubara, F. *J. Phys. Soc. Jpn.* **1982**, *51*, 2424−2432.
(45) Miyashita, S.; Kawamura, H. *J. Phys. Soc. Jpn.* **1985**, *54*, 3385−3395.
(46) Melchy, P. É.; Zhitomirsky, M. E. *Phys. Rev. B: Condens. Matter Mater. Phys.* **2009**, *80*, 064411.
(47) Gvozdikova, M. V.; Melchy, P. E.; Zhitomirsky, M. E. *J. Phys.: Condens. Matter* **2011**, *23*, 164209.
(48) Seabra, L.; Momoi, T.; Sindzingre, P.; Shannon, N. *Phys. Rev. B: Condens. Matter Mater. Phys.* **2011**, *84*, 214418.
(49) Seki, S.; Onose, Y.; Tokura, Y. *Phys. Rev. Lett.* **2008**, *101*, 067204.
(50) Kresse, G.; Hafner, J. *Phys. Rev. B: Condens. Matter Mater. Phys.* **1993**, *47*, 558−561.
(51) Kresse, G.; Furthmüller, J. *Phys. Rev. B: Condens. Matter Mater. Phys.* **1996**, *54*, 11169−11186.
(52) Okuyama, D.; Ishiwata, S.; Takahashi, Y.; Yamauchi, K.; Picozzi, S.; Sugimoto, K.; Sakai, H.; Takata, M.; Shimano, R.; Taguchi, Y.; Arima, T.; Tokura, Y. *Phys. Rev. B: Condens. Matter Mater. Phys.* **2011**, *84*, 054440.
(53) Lu, X. Z.; Whangbo, M. H.; Dong, S.; Gong, X. G.; Xiang, H. J. *Phys. Rev. Lett.* **2012**, *108*, 187204.
(54) Zhang, G.; Dong, S.; Yan, Z.; Guo, Y.; Zhang, Q.; Yunoki, S.; Dagotto, E.; Liu, J. M. *Phys. Rev. B: Condens. Matter Mater. Phys.* **2011**, *84*, 174413.
(55) Johnson, R. D.; Chapon, L. C.; Khalyavin, D. D.; Manuel, P.; Radaelli, P. G.; Martin, C. *Phys. Rev. Lett.* **2012**, *108*, 067201.

DOI: 10.1021/acs.inorgchem.5b02270
Inorg. Chem. 2016, 55, 2709−2716